Metavalent Bonding in Solids: Characteristic Representatives, Their Properties, and Design Options

Yudong Cheng, Sophia Wahl, and Matthias Wuttig*

Heavier chalcogenides display a surprisingly wide range of applications enabled by their unconventional properties. Herein, recent studies of three groups of chalcogenides from a chemical bonding perspective are reviewed to reveal the underlying reason for their wide range of applications. For IV–VI materials (GeTe, SnTe, PbTe, PbSe, and PbS), the unique property portfolio and bond-breaking behavior are related to a novel chemical bonding mechanism termed "metavalent bonding" (MVB). The same phenomena are also found for several V_2VI_3 solids (Bi_2Te_3, Bi_2Se_3, Sb_2Te_3, and β-As_2Te_3) and some ternary chalcogenides including crystalline $(GeTe)_{1-x}(Sb_2Te_3)_x$ alloys. This provides evidence for the prevalence of MVB in these compounds. Subsequently, a quantum-chemistry-based map is presented. Using the transfer and sharing of electrons between adjacent atoms as its two coordinates, materials using MVB are all found in a well-defined region of the map, characterized by sharing about one electron between adjacent atoms and only small charge transfer. This also implies that the degree of MVB is tailored either via Peierls distortions (electron sharing) or charge transfer (electron transfer), leading to the transition toward covalent bonding and ionic bonding, respectively. The tailoring of MVB provides a new approach for materials design.

1. Introduction

Heavier chalcogenides display a surprisingly wide range of applications. GeTe, Sb_2Te_3, and their alloys have been used since the 1980s as phase-change materials (PCMs).[1–3] Initially the focus was on rewriteable optical data storage, but later the usage in electronic memories including storage class memories

Y. Cheng, S. Wahl, Prof. M. Wuttig
Institute of Physics (IA)
RWTH Aachen University
52056 Aachen, Germany
E-mail: wuttig@physik.rwth-aachen.de

Prof. M. Wuttig
PGI 10 (Green IT)
Forschungszentrum Jülich GmbH
52428 Jülich, Germany

The ORCID identification number(s) for the author(s) of this article can be found under https://doi.org/10.1002/pssr.202000482.

motivated significant research activities.[4] At present, this material class is garnering attention for its potential in emerging new technologies like artificial intelligence, neuroinspired computing, or active nanophotonics.[5–9] Applications such as data storage and processing devices rely on a range of technologically important properties in these heavier chalcogenides, including a pronounced optical and/or electrical property contrast, rapid switching speeds, and good thermal stability. Furthermore, compounds like GeTe, PbTe, SnTe, Bi_2Se_3, and Bi_2Te_3 are utilized as thermoelectrics due to the remarkable combination of seemingly contradictory properties. They possess a high Seebeck coefficient like a semiconductor, high electrical conductivity like a metal, and low thermal conductivity like glass.[10–15] Apparently these properties benefit from the effective masses of charge carriers, which are closely related to the metavalent bonding (MVB) mechanism.[16,17]

SnTe, Bi_2Se_3, and Bi_2Te_3 are also investigated for their potential usage as topological insulators, an application benefitting from their unique band structure.[18,19] These diverse applications raise the question of whether there is a common set of material properties, which enables these broad range of applications and how these properties can be explained.

In this Review, we summarize recent results regarding the unconventional properties of three groups of chalcogenides and their origin from a chemical bonding perspective. At first, the unique properties of these families of chalcogenides will be discussed. Five material properties are used as chemical bonding indicators, providing evidence for a bonding mechanism which differs substantially from metallic, ionic, or covalent bonding, as well as the two weaker bonding types of hydrogen and van der Waals. This novel type of bonding has been termed "MVB." The unique properties of some IV–VI materials such as GeTe or PbTe are deeply rooted in this novel chemical bonding mechanism. Subsequently, a number of sesquichalcogenides such as Bi_2Se_3 and Sb_2Te_3 are presented, which possess a similar property portfolio and applications. Finally, it is shown that ternary chalcogenides like $GeSb_2Te_4$ or $Ge_2Sb_2Te_5$ further extend the range of materials which use MVB. Then, a newly developed map is discussed, which is based on advanced quantum chemical calculations. This novel map is able to separate different chemical bonding mechanisms and provides further support for the existence of MVB. This map is spanned by two

**ADVANCED
SCIENCE NEWS**

www.advancedsciencenews.com

pss rrl
physica status solidi

www.pss-rapid.com

coordinates, which quantify the sharing of electrons (electron pair formation) between adjacent atoms and the transfer of electrons between them. Hence, one can ponder how these two quantities can be utilized to tailor material properties. The last section thus focuses on the tailoring of MVB via either distortions (increased electron sharing) or charge transfer (electron transfer), providing attractive opportunities for material design.

2. Prevalence of MVB in Heavy Chalcogenides

2.1. Chemical Bonding Mechanism of IV–VI Solids

As has been well-established for decades, bonding in solids can be classified into five different types, i.e., three "primary bonds" (covalent, ionic, and metallic bonds) and two weaker bonds (hydrogen and van der Waals bonds).[20] For the three primary types of bonding, their valence charges are either localized between two adjacent atoms as electron pairs (covalent), at the ion cores due to pronounced charge transfer (ionic), or are fully delocalized to form an electron cloud (metallic), respectively. The different types of chemical bonds provide a simple but convenient prediction of properties. The delocalized nature of the conductance electrons in metals leads to high electrical conductivity, as evidenced by the success of the Sommerfeld model to explain basic properties of metals. The strong electrostatic attraction between cations and anions due to charge transfer in ionic compounds explains their large bandgap and very low electrical conductivity. For covalent materials, their bandgaps and electrical conductivities are often in between those of metals and ionic compounds. These facts all emphasize an intimate link between bonding types and material properties. Note that some materials may have both covalent and ionic bond contributions, as exemplified by GaN.

Interestingly, crystalline IV–VI compounds such as GeTe or PbTe possess a unique combination of properties which contributes to their wide range of applications including phase change memories and thermoelectrics.[7,8,13–15,17,19] As shown in **Table 1**, the characteristic property portfolio of GeTe is compared with the same properties of materials using ionic, metallic, or covalent bonding. From the comparison in Table 1, GeTe demonstrates a striking difference in properties, which has been attributed to a bonding type which is distinctively different from metallic, ionic, and covalent bonding.[21,22] This rather unconventional combination of properties has also been found in SnTe, PbTe, PbSe, and PbS.[23]

The electrical conductivity, for example, a simple indicator of electron localization/delocalization, is large in metals and small in undoped compounds using ionic or covalent bonding. However, for IV–VI solids such as GeTe, SnTe, or PbTe, they reveal intermediate values approaching the conductivities of bad metals.[21,24,25] Besides electrical conductivity, these materials also possess a unique structural feature as indicated by the effective coordination number (ECoN).[26] The ECoN describes a distance-weighted average over all neighbors and is well-suited to characterize trends in the atomic arrangement for systems which undergo local distortions. For those solids, where the distance to the second nearest neighbor is considerably larger than the one to the nearest neighbors, ECoN resembles the number of nearest neighbors. Typically, for covalent materials like III–V semiconductors, an ECoN ≈ 4 is compatible with the 8–N rule and the sp^3 bonding configuration. For metals, the close packing of atoms usually results in 8 or 12 nearest neighbors. However, for materials like GeTe and SnTe, where atoms are linked by half-filled σ-bonds formed by p-electrons, the rather high ECoNs of 5.2 and 5.94, respectively, are incompatible with the 8-N rule.[21] Such high ECoN values are indicative of a low-valence electron count for adjacent atoms, where about one electron is shared between two atoms. This bonding configuration is in striking contrast to the electron pair used for ordinary covalent bonding. The electronic polarizability of valence electrons as probed by the optical dielectric constant ε_∞ is anomalously high for GeTe and related IV–VI compounds. The chemical bond polarizability, i.e., the response of electronic distribution to distortions as characterized by the Born effective charge Z^*, is also anomalously large.[27,28] Finally, these materials all feature high values of the Grüneisen parameter for transverse optical modes γ_{TO}, a measure of lattice anharmonicity. This property is important for thermoelectric materials as a high γ_{TO} leads to an intrinsically low lattice thermal conductivity.[16,29–31]

These unique combinations of properties of IV–VI compounds like GeTe, SnTe, or PbSe are incompatible with the characteristic properties shown by materials which use metallic, ionic, or covalent bonding. These unconventional properties are also not due to a combination of metallic, ionic, or covalent bonding, as shown from the Grüneisen parameter for example. It is usually small in materials which use metallic or covalent bonding but is large for IV–VI compounds like GeTe or PbTe. Further evidence for an unconventional bonding mechanism comes from atom probe tomography (APT). In this technique, laser-assisted field evaporation is utilized to decompose a sample

Table 1. Five properties to differentiate the chemical bonding mechanisms (cf. ref. [22]).

Bonding property identifier	Ionic (e.g., NaCl)	Covalent (e.g., Si)	Metavalent (e.g., GeTe)	Metallic (e.g., Cu)
Electronic conductivity (electrical identifier)	Very low ($< 10^{-8}$ S cm^{-1})	Low to moderate (10^{-8}–10^2 S cm^{-1})	Moderate (10^1–10^4 S cm^{-1})	High ($> 10^5$ S cm^{-1})
ECoN (structural identifier)[a]	4(ZnS), 6 (NaCl), 8 (CsCl)	8-N rule satisfied	8-N rule not satisfied	8 (bcc) 12 (fcc/hcp)
Optical dielectric constant (optical identifier)	Low ($\approx$2–3)	Moderate ($\approx$5–15)	High ($>$15)	—[b]
Born effective charge (chemical bond polarizability)	Low (1–2)	Moderate (2–3)	High (4–6)	Vanishes (0)
Grüneisen parameter (anharmonicity)	Moderate (2–3)	Low (0–2)	High ($>$3)	Low (0–2)

[a]For ionic and metallic systems, representative structure types are given, but there are many others especially for multinary systems (e.g., in Zintl phases); [b]Not normally applicable to the metallic state.

ADVANCED SCIENCE NEWS
www.advancedsciencenews.com

pss rrl
physica status solidi
www.pss-rapid.com

with nearly atomic resolution.[32] A characteristic of this process is the probability to create more than one ion (fragment) upon one successful laser pulse.[32] This quantity, which is called the probability to create multiple events (PME), is much higher for materials such as GeTe or PbSe, compared with GeSe or SnSe.[33] All of these findings suggest the bonding in the corresponding IV–VI compounds to be distinctively different from covalent, metallic, and ionic bonding. Indeed, already in the 1970s and 1980s, some of the unconventional properties were noted and attributed to "resonant bonding" by Lucovsky and White and later Littlewood.[27,34,35] Later some of us also noted that many PCMs possess properties which were attributed to "resonant bonding" in the case of GeTe.[28,36] The concept of "resonant bonding" was introduced even long before by Pauling.[20] Since then, it has been widely used to explain the atomic arrangement and structure of organic compounds like benzene using a valence-bond framework.[20] However, it has recently been shown that the properties of benzene, graphene, and graphite differ significantly from those shown for the IV–VI compounds discussed here (GeTe, SnTe, PbTe, PbSe, PbS).[21] The same holds for the characteristics of bond breaking as revealed by ATP, which shows striking differences between the IV–VI compounds mentioned earlier, and graphene sheets, which behave like covalently bonded materials in terms of their bond rupture.[37] Hence, the name "resonant bonding" should be abandoned for monochalcogenides. Instead, a new name, i.e., MVB, has been proposed to highlight the uniqueness of this novel bonding mechanism and fundamentally differentiate it from metallic, ionic, and covalent bond types but also resonant bonding, as shown in materials like benzene.[21,38]

2.2. Bonding Mechanism of V_2VI_3 Solids

Interestingly, besides the IV–VI compounds discussed earlier, another group of chalcogenides (V_2VI_3 solids, i.e., sesquichalcogenides) is also known for their wide range of applications.[7,11,18,39,40] The similarity of their applications as compared with the IV–VI compounds immediately raises one question: can the similarity of material properties and applications be explained by the prevalence of the same type of bonding? Recently, the bonding mechanism in a variety of V_2VI_3 compounds has been investigated using different characterization techniques including APT and density functional theory (DFT) calculations.[41]
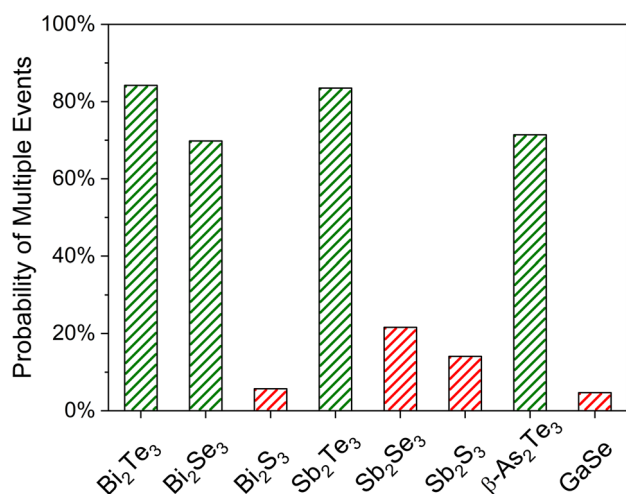
Several characteristic properties of V_2VI_3 solids are shown in **Table 2**, including the electrical conductivity σ, the normalized Born effective charges Z_n^*, the ECoN, and the optical dielectric constant ε_∞ along different directions. Z_n^* values are averaged over atoms and directions. ε_∞ reveals different values along different directions due to the anisotropy of the noncubic structure. In addition, the Debye temperature (θ_D) is also given to characterize the bond stiffness. Table 2 shows a striking difference between two sets of sesquichalcogenides. The properties of the four sesquichalcogenides (Bi_2Te_3, Bi_2Se_3, Sb_2Te_3, and β-As_2Te_3) resemble the properties of GeTe,[41] whereas three others behave quite different (Bi_2S_3, Sb_2Se_3, and Sb_2S_3). This difference is most obvious for the electrical conductivity shown in Table 2. The electrical conductivity of undoped materials at room temperature is a good measure of the delocalization or localization of electrons. It is high in metals whose valence electrons are fully delocalized and low in undoped ionic or covalent materials whose valence electrons are localized. However, Bi_2Te_3, Bi_2Se_3, Sb_2Te_3, and β-As_2Te_3 have intermediate conductivity values. Their conductivities are several orders of magnitude higher than the other three V_2VI_3 solids but slightly lower than those of metals. A similar behavior has also been observed for the IV–VI (GeTe: $\approx 5.0 \times 10^3$; GeSe: $\approx 1.30 \times 10^{-6}$) solids discussed earlier whose electronic transport properties are almost metal like.[21,42,43]

Besides the electrical conductivity, also other physical properties shown in Table 2, i.e., the normalized Born effective charge Z_n^*, the optical dielectric constant (ε_∞), and the Debye temperature (θ_D), clearly separate all V_2VI_3 materials into two groups. The Born effective charge Z^* provides a measure of chemical bond polarizability. For an ionic bond, the normalized Born effective charge Z_n^* resembles the nominal ionic charge,[44] i.e., the formal oxidation state of the ions involved. For example, Z^* is close to 1 for the ion cores in NaCl and about 2 for MgO, and their Z_n^* values are both close to 1.[45,46] Hence, to facilitate the comparison, we consider the normalized Born effective charge Z_n^*, obtained after dividing Z^* by the oxidation state. As shown in Table 2, the normalized Born effective charges Z_n^* are anomalously large for Bi_2Te_3, Bi_2Se_3, Sb_2Te_3 and β-As_2Te_3 and clearly exceed the values of Bi_2S_3, Sb_2S_3, and Sb_2Se_3. Similar trends are also observed for ε_∞ and ECoNs. The ε_∞ values perpendicular to the layers in Bi_2Te_3, Bi_2Se_3, Sb_2Te_3, and β-As_2Te_3 are smaller than the in-plane components. This is due to the weaker coupling across the van der Walls-like gaps as compared with the coupling within the layers. Yet, even for the optical polarizability in z-direction, the highest values are found for the same four compounds. Regarding the ECoN, like in GeTe, both the shorter and longer bonds in V_2VI_3 compounds are taken into account. Finally, the lower Debye temperatures observed for Bi_2Te_3, Bi_2Se_3, Sb_2Te_3, and β-As_2Te_3 are indicative of soft bonds. All of these properties are characteristic for the unconventional bonding mechanism found for GeTe, i.e., MVB. The results presented earlier imply that MVB also prevails in V_2VI_3 systems such as Bi_2Te_3, Bi_2Se_3, Sb_2Te_3, and β-As_2Te_3.

To further confirm the prevalence of MVB in Bi_2Te_3, Bi_2Se_3, Sb_2Te_3, and β-As_2Te_3, APT was used to analyze these compounds and characterize the bond-breaking behavior, using the PME.[41] This PME quantifies the probability of dislodging more than one

Table 2. Various properties of V_2VI_3 materials.[41] The normalized Born effective charges Z_n^*, ECoN, bandgap (E_g), and the diagonal elements of the optical dielectric constant tensor (ε_∞) are determined by DFT calculations. Reference values for the electrical conductivities and Debye temperatures are also given.

	σ [S cm^{-1}]	Log σ	Z_n^*	ECoN	E_g [eV]	ε_∞	θ_D [K]
Bi_2Te_3	6.6×10^2	2.82	2.06	5.79	0.53	(35.4; 35.4; 25.5)	155
Bi_2Se_3	1.0×10^3	3.00	1.66	5.66	0.54	(19.8; 19.8; 12.0)	182
Bi_2S_3	2.0×10^{-3}	−2.69	1.63	4.76	1.36	(14.0; 14.1; 9.7)	284
Sb_2Te_3	2.3×10^3	3.36	1.98	5.84	0.29	(39.5; 39.5; 24.7)	162
Sb_2Se_3	4.0×10^{-7}	−6.40	1.47	4.17	0.76	(19.1; 18.5; 9.7)	292
Sb_2S_3	1.0×10^{-8}	−8.00	1.41	3.92	1.28	(14.2; 12.5; 7.34)	364
β-As_2Te_3	6.5×10^2	2.81	2.47	5.84	0.26	(65.7; 65.7; 42.6)	148

ADVANCED
SCIENCE NEWS
www.advancedsciencenews.com

pss rrl
physica status solidi
www.pss-rapid.com

Figure 1. Probabilities of the formation of multiple events for seven V_2VI_3 compounds and GaSe as revealed by APT. Only Bi_2Te_3, Bi_2Se_3, Sb_2Te_3, and β-As_2Te_3 show a high probability to form multiple events, whereas Bi_2S_3, Sb_2S_3 and Sb_2Se_3, and GaSe are characterized by a low PME during APT measurements. Reproduced with permission.[41] Copyright 2019, The Authors, published by Wiley-VCH.

ion when a successful laser pulse is applied to a needle-shaped specimen. A small but not-zero PME is always observed during APT measurements of metals and covalently bonded semiconductors like Si and GaAs.[33] This is in striking contrast to GeTe, where a unique bond-breaking behavior, i.e., very high PME, is observed.[33] Surprisingly, as shown in **Figure 1**, an unconventional and characteristic pattern of bond rupture has also been found for the four V_2VI_3 compounds. It closely resembles the bond rupture shown in GeTe and is indicative for the same bonding mechanism. On the contrary, Bi_2S_3, Sb_2S_3, and Sb_2Se_3 show an ordinary bond rupture, as also observed for covalently bonded materials like GaAs or Si. We hence observe the same striking difference in bond rupture that was already noted for the material properties.

This conclusion is actually puzzling at first glance considering the atomic arrangement of the four compounds Bi_2Te_3, Bi_2Se_3,

Sb_2Te_3, and β-As_2Te_3. All four show a similar rhombohedral structure, consisting of quintuple layers separated by vacancy layers, see the left panel of **Figure 2**. These vacancy layers have been described as van der Waals gaps linked by weak van der Waals bonds. In typical 2D solids like GaSe (see the right panel of Figure 2), covalent bonds prevail inside adjacent blocks, which are separated by van der Waals gaps. As the van der Waals interaction is rather weak compared with covalent bonding, the electrons are mainly localized inside the building stacks, and the electron density inside van der Waals gaps is very low. Therefore, sesquichalcogenides are frequently discussed as 2D solids, comparable with graphene or transition metal dichalcogenides.[47] However, the presence of van der Waals gap is incompatible with the concept of MVB. MVB is an electronic interaction beyond the first nearest neighbors, but instead extends to an intermediate length scale, so that also more distant neighbors contribute significantly.[21,29,48,49] This implies that the nature of the vacancy layers in Bi_2Te_3, Bi_2Se_3, Sb_2Te_3, and β-As_2Te_3 needs to be carefully considered.

We know that there is a close correlation between interatomic distance and bond strength. Hence, a simple bond length–bond strength correlation is utilized to compare the interlayer coupling between two chalcogenide atoms, i.e., the "Te–Te" or "Se–Se" interaction in different solids, as in Figure 2. After normalizing the interatomic distances to the expected van der Waals bond lengths (the sum of the van der Waals radii of the two constituents), the interlayer distances are shown in Figure 2. For a typical 2D solid such as GaSe, the interatomic distance between two adjacent Se atoms crossing a van der Waals gap is 2.9% longer than the theoretical value. On the contrary, for the four chalcogenides Bi_2Te_3, Bi_2Se_3, Sb_2Te_3, and β-As_2Te_3, the interatomic distances between two quintuple layers are considerably shorter than the expected values for van der Waals bonds. This is indicative for a considerably stronger electronic coupling across the vacancy layers and hence an additional energetic contribution besides weak van der Waals bonding. In addition, we can use the number of interlayer electrons sharing (ES), as calculated in a study by Cheng et al.[41], as another quantifier of the strength of this coupling. For GaSe, the ES between adjacent Se atoms across van der Waals gaps is as
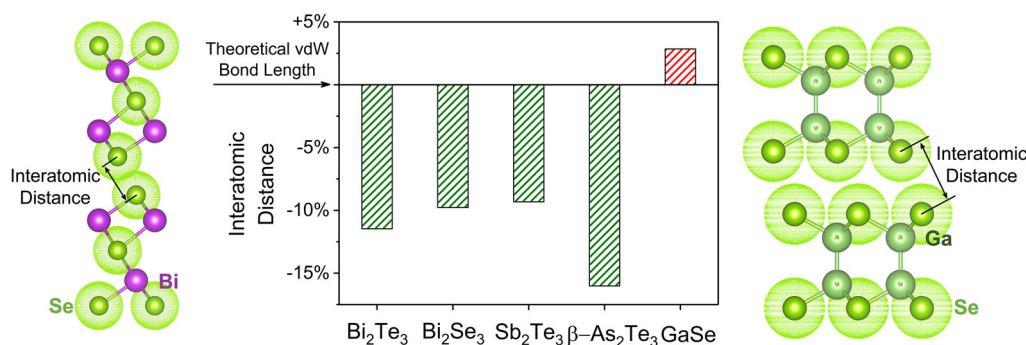
Figure 2. Interatomic distance between adjacent chalcogenide atoms across the van der Waals-like gap. The actual distance is normalized to the expected van der Waals bond length. The interatomic distances of Bi_2Se_3 (left) and GaSe (right) and the expected van der Waals bond length are sketched, where the green circles denote the van der Waals radius of Se. Note that the atomic size is not drawn to scale. For GaSe, the interlayer bond length is 2.9% longer than the expected value. However, on the contrary, the significantly shortened (−10% to −15%) interlayer interatomic distances of Bi_2Te_3, Bi_2Se_3, Sb_2Te_3, and β-As_2Te_3 suggest that a stronger electronic coupling is incompatible with real van der Waals gaps. Reproduced with permission.[41] Copyright 2019, The Authors, published by Wiley-VCH.

low as 0.04 e, in line with the expected weak van der Waals bonds. Instead, the corresponding numbers are much higher for the four sesquichalcogenides which show a distinct property portfolio: Bi_2Te_3 (0.272 e), Bi_2Se_3 (0.132 e), Sb_2Te_3 (0.244 e), and β-As_2Te_3 (0.192 e). This pronounced electron sharing across the gap is indicative for strong electronic coupling between adjacent quintuple layers. It is interesting to ponder if this strong coupling across the gap is a prerequisite to establish MVB in the sesquichalcogenides.

2.3. Bonding Mechanism of Ternary Chalcogenides

The prevalence of MVB in IV–VI and V_2VI_3 binary chalcogenides is potentially also interesting to unravel the origin of the unconventional properties of PCMs. The mono- and sesquichalcogenides are the "parent compounds" of many ternary chalcogenides, including Ge–Sb–Te alloys (GSTs) on the GeTe–Sb_2Te_3 pseudobinary line. Compounds such as $Ge_2Sb_2Te_5$ are widely used in phase change memory applications. The pronounced optical and electrical contrast between the amorphous and crystalline state has been attributed to a change of the bonding mechanism, i.e., from covalent bonding in the amorphous state to MVB in the crystalline state.[36,50]

As one of the characteristic properties of MVB solids, the optical dielectric constant of the crystalline state is much higher than the corresponding amorphous state, indicative of a high electronic polarizability.[36] The real part of the dielectric function and the optical dielectric constants for various chalcogenides (both for the crystalline and for the amorphous state) are shown in **Figure 3**. Clearly, the pronounced optical contrast and the anomalously high optical dielectric constant persist in all $(GeTe)_{1-x}$–$(Sb_2Te_3)_x$ compounds studied. Besides the optical identifier, also the coordination numbers of crystalline GSTs differ significantly from their amorphous counterparts. While crystalline PCMs have values very close to the value for an ideal octahedral structure ($\approx$6), the amorphous states have much lower values ($\approx$4).[51] Hence, the bond order in crystalline GSTs is also much smaller than 1, as only about one p-electron is shared by two atoms. Instead, it is much closer to 1/2. Hence, the combination of high coordination numbers and low bond orders characterizes a situation, where the distortions are small and the bonds are weak. This might explain partly as to why the bond breaking as seen by APT is characterized by high
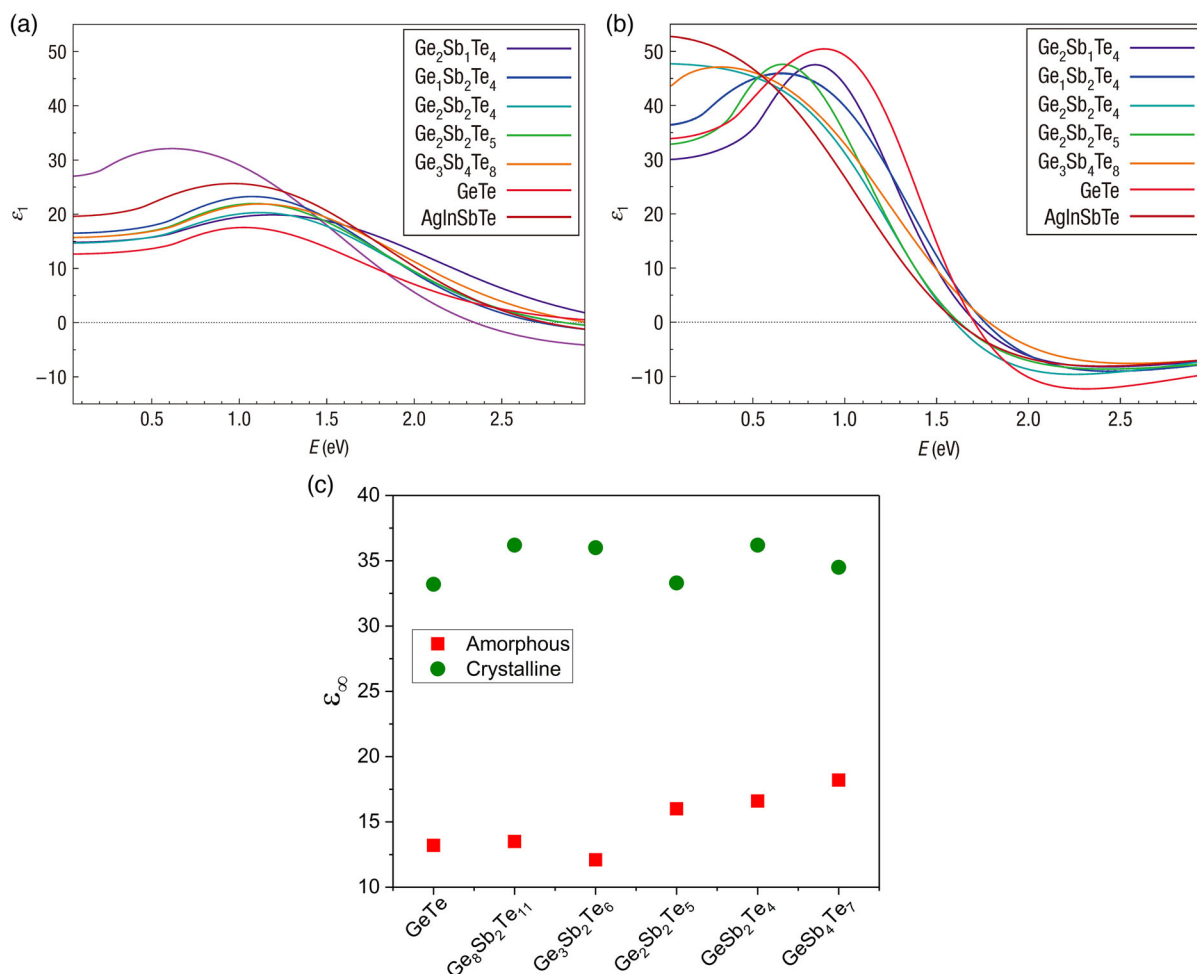

Figure 3. The real part of the dielectric functions for various PCMs. a) Amorphous state. b) Crystalline state. c) The optical dielectric constants of various $(GeTe)_{1-x}$–$(Sb_2Te_3)_x$ alloys (data are taken from ref. [93]). Reproduced with permission.[36] Copyright 2008, Springer Nature.

probabilities of multiple events.[33] The concept of MVB can thus be extended from IV–VI compounds such as GeTe, SnTe, PbTe, PbSe, and PbS to V_2VI_3 compounds, including Bi_2Te_3, Bi_2Se_3, Sb_2Te_3, and β-As_2Te_3 and finally to ternary chalcogenides (like $GeSb_2Te_4$ or $Ge_2Sb_2Te_5$).

2.4. An Electronic Map for Bonding Mechanisms

MVB has initially been introduced to explain an unconventional combination of material properties. Subsequently, the unusual bond breaking observed by APT provided further support for this novel type of bonding. Finally, the development of quantum chemical computations provides a quantitative tool to characterize chemical bonding. Recently, a quantum-mechanical-based electronic map for bonding in solids was introduced, which is based on two quantum mechanical coordinates: the electron sharing (ES) and electron transferred (ET) between two neighboring atoms.[38] To obtain the number of ES and ET, Bader's basins

(Ω) are first defined for each atom in the unit cell. The electron transfer is determined by integrating the net charge density of an atom over its basin and subtracting the charge of the free reference atom. The electron sharing is evaluated with the so-called delocalization indices that are computed at the two-electron level of theory. They are deduced from the analysis of the electron pair density over the relevant basins. An electron sharing between neighbouring atoms equal to 2 would correspond to the Lewis picture of a perfect covalent bond, i.e., an electron pair. More details can be found in a study by Raty et al.[38] The map based on these two coordinates is capable of separating different bonding mechanisms, see **Figure 4**a. Note that, instead of the total number of electrons being transferred,[38] the renormalized electron transfer is chosen here, which is obtained by dividing the absolute electron transfer by the oxidation state of the corresponding atom.[41] Please note that for the determination of the number of ES, an ECON averaged number is calculated, which also includes longer distances, but weighs those with an exponential decay.
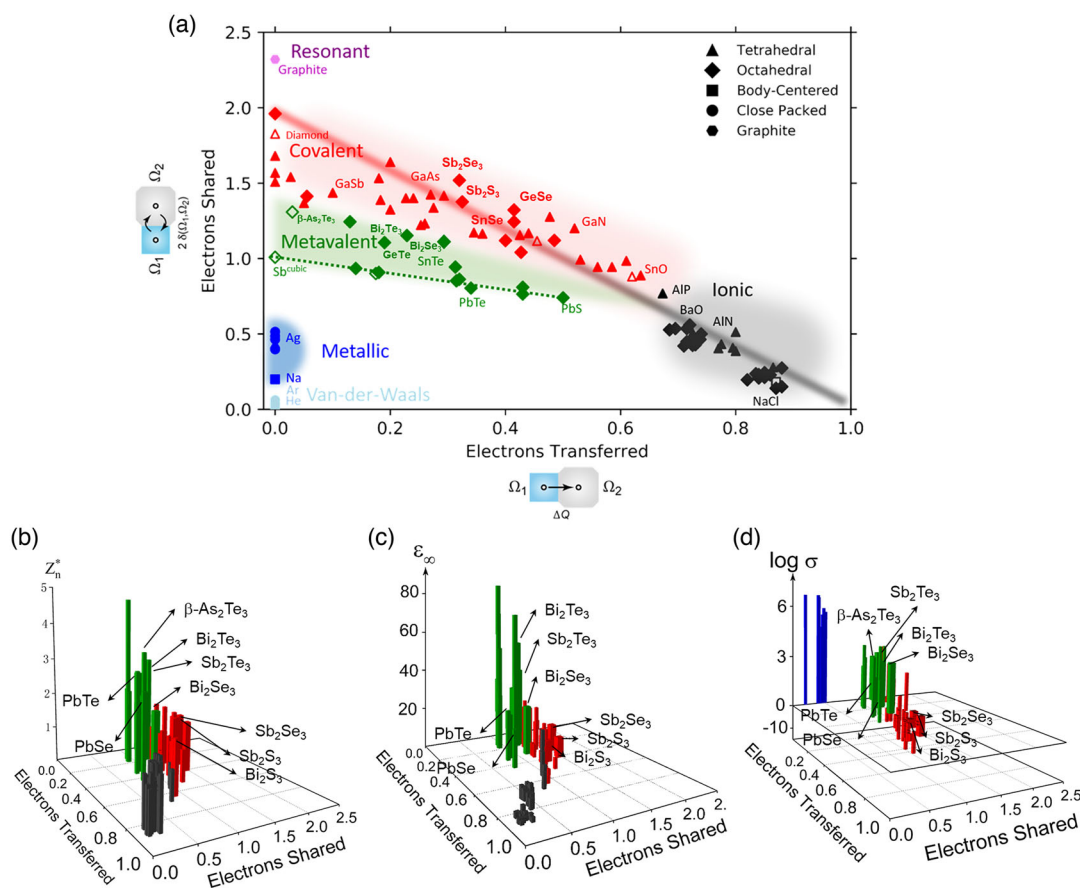
Figure 4. a) The 2D map describing bonding in various solids. The map is spanned by the electron transfer and the sharing of electrons between adjacent atoms. Triangles, diamonds, squares, and circles denote tetrahedrally bonded solids, distorted and ideal rocksalt-type (octahedrally coordinated) structures, body-centered solids, and close-packed metals, respectively. Filled and open symbols represent thermodynamically stable and metastable phases. b–d) The 2D map is then extended in the third dimension using three independent properties, i.e., the normalized Born effective charge Z_n^*, the optical dielectric constant ϵ_∞, and the electrical conductivity σ, displayed as log σ. Black, red, blue, and green describe materials which utilize predominantly ionic, covalent, metallic, and MVB, respectively. Clearly, MVB compounds are characterized by anomalously high values of all three indicators, not found for materials which use one of the other bonding mechanisms. All solids with an ideal rocksalt structure and half-filled σ-bonds of p-orbitals are located on the dashed green line. Distorted octahedral structures with similar numbers of p-electrons involved in bond formation are characterized by a higher number of ES. a) Reproduced with permission.[22] Copyright 2020, The Authors, published by Wiley-VCH. b–d) Reproduced with permission.[41] Copyright 2019, The Authors, published by Wiley-VCH.

ADVANCED SCIENCE NEWS
www.advancedsciencenews.com

pss rrl
physica status solidi
www.pss-rapid.com

Hence, also the second nearest neighbors are included for distorted structures.

The map clearly separates ionic, covalent, and metallic bonding. Materials which use ionic bonding, such as NaCl or MgO, are located in the lower right corner of the map, which characterizes compounds with significant electron transfer but minor sharing of electrons between adjacent atoms. Solids like Si are characterized by a high degree of electron sharing, approaching the value of 2 expected for an electron pair, and are thus located in the upper left corner of the map. Several van der Waals-bonded solids can be found in the bottom left corner, characterized by vanishing electron transfer and marginal electron sharing. Metallic bonding, as found in Al, Na, or Ag, is characterized by small electron transfer and moderate electron sharing. Interestingly, resonantly bonded materials like graphite are found in a separate region of the map, characterized by the very significant sharing of electrons between adjacent atoms. This can be explained by the coexistence of a covalent bond (an electron pair) and an additional electron between two adjacent atoms, providing an additional bond order of 1/2. Hence, all five bonding mechanisms discussed so far are located in clearly separated regions of the map. The only two bonding mechanisms with ill-defined borders are ionic and covalent bonding. This is a reflection of common knowledge that the transition between these two bonding mechanisms seems rather continuous, i.e., apparently lacking a well-defined "border".

Interestingly, all chalcogenides discussed so far fall into two separate regions of the map. More specifically, GeSe, SnSe, SnS, Bi_2S_3, Sb_2Se_3, and Sb_2S_3 are all located in a region, where other covalently bonded materials such as InSb, Si, or ZnSe are found. GeTe, SnTe, PbTe, PbSe, Bi_2Te_3, Bi_2Se_3, Sb_2Te_3, and β-As_2Te_3, instead, can be found in a separate region. This region is characterized by about one electron being shared and a modest level of electron transfer, consistent with the half-filled σ-bonds of p-orbitals discussed earlier. These two regions do not overlap. Instead, they seem to exhibit a discontinuous border as evidenced by APT measurements.[33]

Finally, the map can be extended to a third dimension using material properties, such as the Born effective charge, the dielectric constant, or the electrical conductivity, as shown in Figure 4b–d. In all three maps, the properties of materials using MVB stand out and differ clearly from the properties shown by materials displaying other bonding mechanisms. The unusual properties, the unique electronic structure, and the unconventional bond rupture all support the view that MVB is a fundamental and novel bonding mechanism and not a superposition of other bonding mechanisms.

3. Tailoring MVB

MVB has been attributed to σ-bonds predominantly formed by p-electrons. The contribution of s-electrons is very weak due to the large energy differences of s- and p- orbitals.[28,52,53] These ppσ-bonds are half filled, in contrast to the electron pairs forming covalent bonds. These bond-forming p-electrons are neither fully localized as in ionic or covalent bonding, nor fully delocalized as in metallic bonding. Instead, they are characterized by a competition between electron delocalization (metallic

bonding) and electron localization (ionic or covalent bonding). The simplest representative of this bonding mechanism is hypothetic cubic Sb. It has an ECoN of 6 and a bond order of 1/2, i.e., one single electron is shared between two adjacent atoms as only three p-electrons per atom can be utilized to form six bonds to the neighboring atoms. This is consistent with the quantum chemical calculations, which reveal that one electron, i.e., half an electron pair, is shared between adjacent atoms, as shown Figure 4a. This electronic configuration is similar for other MVB materials such as GeTe, SnTe, or PbTe. With two p-electrons from the group-IV element and four p-electrons from the group-VI element, on average, three p-electrons per atom are available in IV–VI solids. For example, six p-electrons of SnTe are used to form six σ-bonds between adjacent atoms (see the ECoN of SnTe).

How can systematic trends be described within the family of metavalently bonded materials? The map implies that there are two options to modify MVB. We can either "move right" to the ionic region or we can move vertically, i.e., either up or down. If we "move up" toward the covalent region, changes of structure and properties are expected. Compounds utilizing half-filled ppσ-bonds should give rise to an ideal octahedral structure and metal-like properties with no bandgap. However, this electronic configuration is energetically unstable. The electronic energy can often be reduced by a structural distortion, i.e., Peierls distortion, which opens a bandgap at the Fermi energy.[54–56] The Peierls distortion produces three shorter and three longer bonds and reduces the ECoN. This increases the number of ES between adjacent atoms.[38,49] Above a certain magnitude of Peierls distortion, apparently, MVB is no longer the most stable type of bonding, and a transition to covalent bonding is observed.[38] Yet, there is a second mechanism, how a bandgap can open.[57] The energy of the solid can also be reduced by charge transfer (moving to the right side in the map). This will also affect the MVB character but leads to a transition toward ionic bonding. Interestingly, in this case, no Peierls distortion occurs and the ECoN remains six until the border to ionic bonding is crossed.

How does this perspective help us to modify material properties? As solids using MVB possess many technically important properties and a wide range of applications, understanding how to change the MVB character will not only benefit our scientific knowledge of bonding mechanisms, but also add one more option to our toolbox of materials design, i.e., bond tailoring. For instance, the character of MVB has been reported to play a significant role in many properties like the photoexcited instantaneous optical change and the soft phonon mode.[31,58–63] Huang and Robertson revealed that MVB in crystalline PCMs is the origin of the optical contrast between the amorphous and crystalline states.[50] The disappearance of MVB has also been demonstrated to be detrimental to the power factor of thermoelectric materials.[17] Therefore, in this section, the two routes of MVB tailoring via electron sharing and electron transfer, i.e., "moving up" and "moving right," and their consequences on material properties will be sketched.

3.1. Chemical Bonding Tailoring via Electron Sharing

As discussed earlier, the half-filled ppσ-bond is energetically unstable, and the Peierls distortion is one way to minimize

ADVANCED
SCIENCE NEWS
www.advancedsciencenews.com

physica
pss status solidi rrl
www.pss-rapid.com

the electronic energy. This leads to two consequences: 1) the actual structure deviates from an ideal octahedral arrangement. Instead, an octahedral-like "3 + 3" coordination is created, forming three short and three long bonds;[49,54,55] 2) the Peierls distortion also leads to the change of the electronic configuration: valence charges gradually transfer from long bonds to short bonds and get more localized.[38] This effect has been investigated by DFT calculation for GeTe.[38] As shown in **Figure 5**a, by manually varying the degree of distortion (represented by the long bond-to-short bond ratio r_l/r_s), Peierls distortion induces the redistribution of electrons between short and long bonds in GeTe. More valence electrons are shared at the shorter bonds although the total number of bond-forming electrons is constant. On the contrary, Peierls distortion does not affect the level of electrons transfer.[38] This enhanced electron sharing is also clearly visible in the map where all ideal rocksalt structures utilizing half-filled σ-bonds are located on one straight line (the green dashed line in Figure 4a), whereas all distorted octahedral structures feature a higher count of ES. The degree of distortion severely impacts the bonding character and finally leads to the transition from MVB to covalent.[38] This explains the pronounced difference in bonding mechanisms and properties between GeTe and SnTe on the one side and GeSe and SnSe on the other side.[21]

Modifying the bonding character via distortions has pronounced effects on many properties. DFT calculations have demonstrated the reduction of Born effective charges and changes of atomic arrangement as reflected by the decreasing ECoNs upon increasing the number of ES, as shown in Figure 5b.[38] In addition, Peierls distortion also has a significant influence on electrical conductivity due to the opening of a bandgap. The bandgap increases with the size of distortion, leading to a decrease in resulting electrical conductivity. **Figure 6** shows the intrinsic electrical conductivity of a variety

of compounds at room temperature, showing the possible link between electrical conductivity and the type of bonding. While good metals such as Ag or Cu have values close to $6 \times 10^5 \, \text{S cm}^{-1}$, an undoped semiconductor such as Si has a conductivity of $3 \times 10^{-8} \, \text{S cm}^{-1}$ at room temperature. Interesting enough, MVB solid materials all fall in a narrow range of conductivities between 1×10^2 and $1 \times 10^4 \, \text{S cm}^{-1}$. This picture is compatible with the small bandgap opened by the weak Peierls distortion. Note that rocksalt structures (SnTe, PbTe, PbSe, and PbS) are also shown in Figure 6, although their transport properties are mainly dominated by electron transfer and not an increase in the number of ES.[23] The almost metal-like electrical conductivities justify calling these materials "incipient metals."[21] Instead, heavily distorted materials such as Bi_2S_3, Sb_2Se_3 and Sb_2S_3, and GeSe and SnSe, where $r_l/r_s \approx 1.2$, are all characterized by a larger bandgap and rather low conductivity.

Interestingly, the electrical conductivities of these MVB compounds are very close to the Mooij rule for bad metals, which identifies the critical conductivity where the temperature coefficient of resistivity changes the sign in metals.[25,64] **Figure 7** shows the correlation between the electronic transport behavior and the degree of distortions in a few p-bonded materials. A metallic behavior (the positive temperature coefficient of resistivity) is found for all weakly distorted materials using MVB, whereas other materials behave like insulators.[64] The transition from Sb_2Se_3 to Bi_2Se_3 has also been reported to show an insulator to metal transition.[65] Actually, the potential link between the degree of distortion and electronic transport properties is also hidden in the value of ECoN as the deviation from an ideal rocksalt-like structure can be characterized by an ECoN value < 6. This raises the question of whether there is a link between MVB and metallic behavior, as reflected for example in the positive temperature coefficient of resistivity. While the question
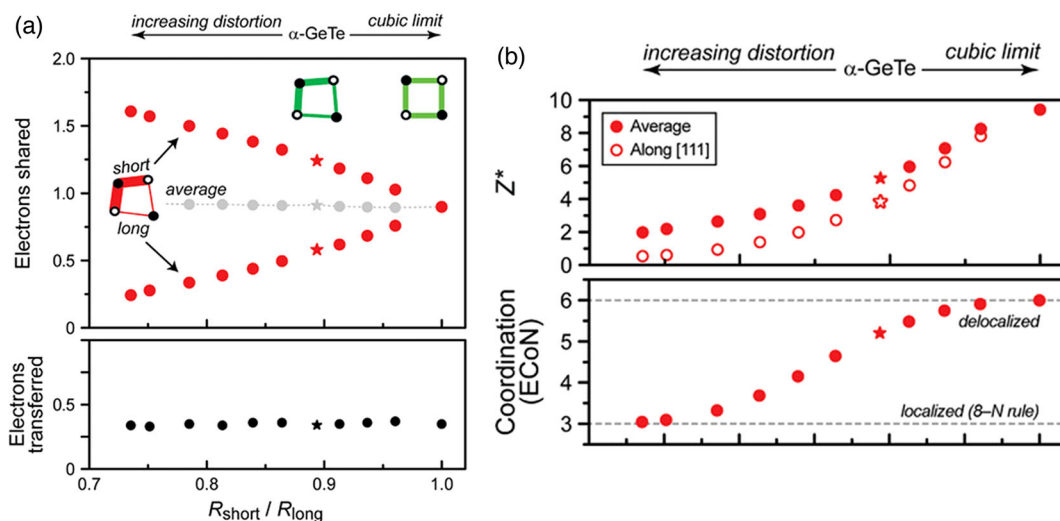

Figure 5. a) The number of ES and ET of a series of GeTe structures that are gradually distorted along [111] direction. The degree of Peierls distortion is quantified through the ratio of shorter and longer interatomic distances, i.e., r_l/r_s. The atomic sketches indicate the redistribution of electron sharing. b) Two different bonding characteristic properties are significantly affected by the degree of Peierls distortion. The upper panel shows the averaged Born effective charges and projected values on the [111] direction; the lower panel shows the change of the ECoN. a,b) Reproduced with permission.[38] Copyright 2019, RWTH Aachen University, published by Wiley-VCH.
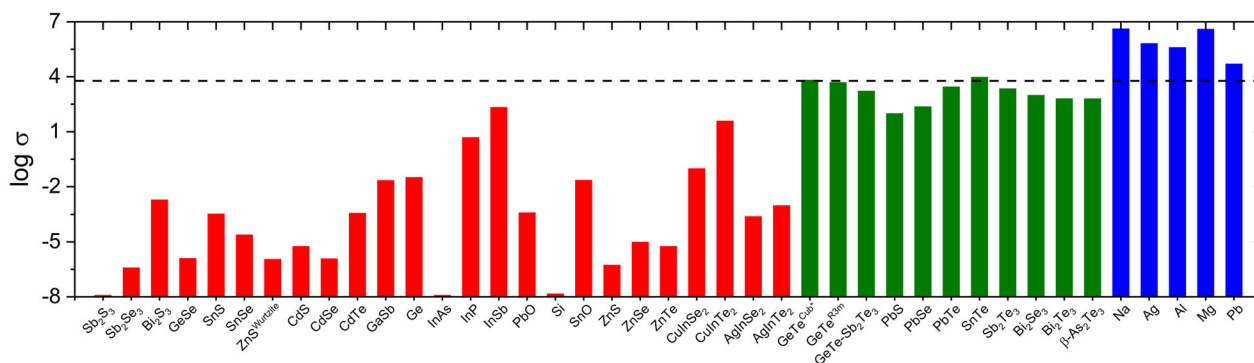
Figure 6. The electrical conductivity data of some representative covalently (red) and metallically bonded (blue) materials, compared with materials using MVB (green). To maximize the clarity of the viewgraph, we restrict the conductivity range between 10^7 S cm^{-1} (good metals such as Ag) and 10^{-8} S cm^{-1} (pure intrinsic semiconductors such as Si) at room temperature. Materials utilizing MVB all fall into a narrow range of conductivities close to the Mooij value of about 6×10^3 S cm^{-1} (dashed line) for bad metals.[25] Room-temperature conductivity values for CuInSe$_2$, CuInTe$_2$, AgInSe$_2$, and AgInTe$_2$ are taken from other studies.[94–97] Reproduced with permission.[41] Copyright 2019, The Authors, published by Wiley-VCH.
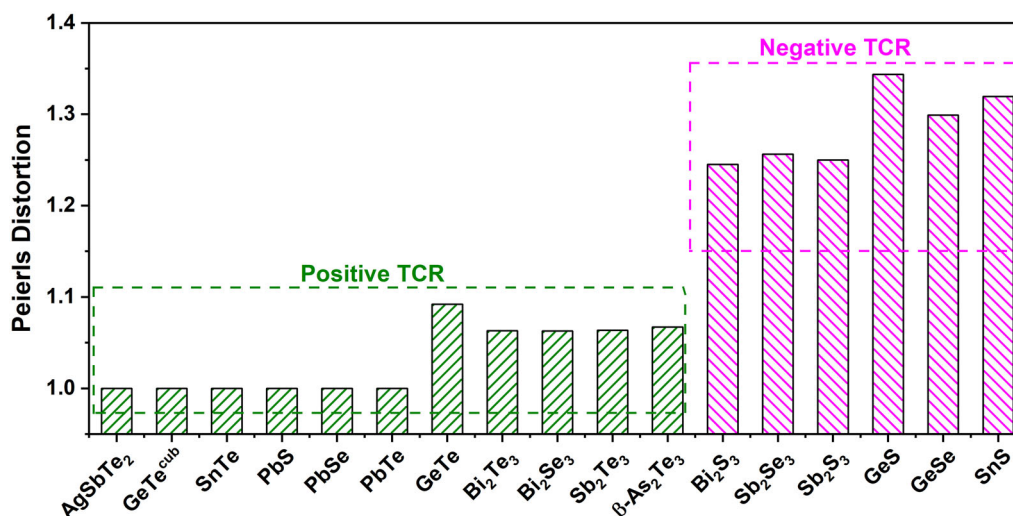

Figure 7. The correlation between the electronic transport behavior and the degree of distortions. The degree of distortion is parameterized by the ratio between the long bond and the short bond. Weak distortions prevail in MVB materials whereas the others are more heavily distorted. The positive temperature coefficient of resistivity (TCR) in weakly distorted MVB materials is evidence for an almost metallic behavior. MVB materials are hence "incipient metals." Data taken from studies by Kooi et al. and Jovovic et al.[22,98] Reproduced with permission.[22] Copyright 2020, The Authors, published by Wiley-VCH.

cannot be fully answered by present results, the interplay between chemical bonding and electronic transport properties deserves further investigations.

3.2. Chemical Bonding Tailoring via Electron Transfer

Previous studies[21,28,38,41,49] and the arguments presented here have provided convincing evidence that changing the degree of electron sharing via distortions has significant consequences for many physical properties. This section will demonstrate that changing the degree of electron transfer also enables the systematic tailoring of the bonding character and many properties. This mechanism has been systematically studied in a subgroup of IV–VI materials, i.e., PbX (X = Te, Se, S, O).[23]

In the map, MVB is located in the region between covalent, metallic, and ionic bonding. Materials using MVB are characterized by moderate electron transfer. The three lead chalcogenides PbTe, PbSe, and PbS all possess the same rocksalt crystal structure. They lie on a straight line in the map within the metavalent region but with apparently a different degree of electron transfer. When going from PbTe to PbS, the charge transfer between cations and anions gradually increases without any structural transition, as evidenced by the identical ECoN in the three solids, as shown in **Figure 8**d. The increasing electron transfer has several important consequences. As shown in Figure 8a, it leads to a decreasing chemical bond polarizability Z_n^*, i.e., the charges become more localized and the bonds become less polarizable. Similar behavior is also found for other material properties such
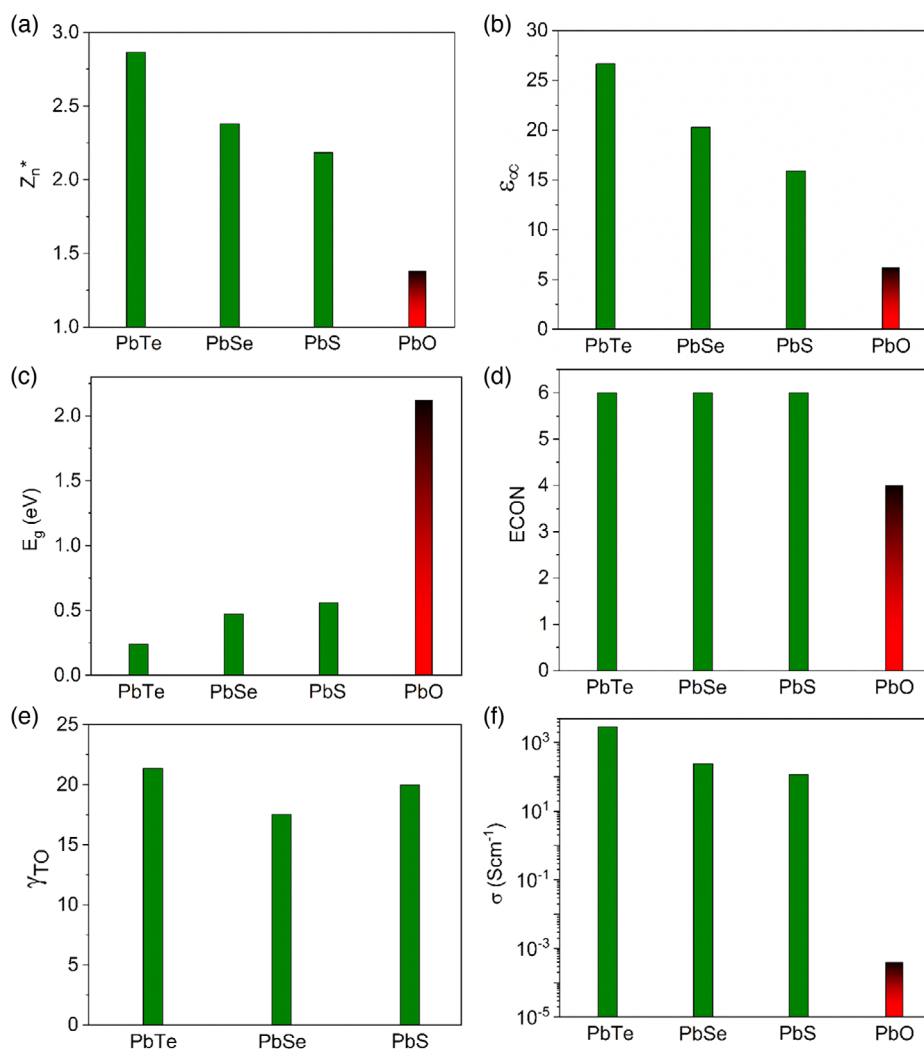
Figure 8. a) Normalized Born effective charge Z_n^*, b) optical dielectric constant, c) optical bandgap, d) ECoN of Pb, e) mode-specific Grüneisen parameter, and f) electrical conductivity of PbX (X = Te, Se, S, O). Clearly, the properties of β-PbO differ substantially from the three higher lead chalcogenides. The green and red colors are indicative of the bonding mechanism of different solids, where green represents MVB whereas the black/red color characterizes iono–covalent bonding. The term "iono–covalent bonding" is utilized to describe the fact that the bonds in this region possess both covalent and ionic bond contributions. Reproduced with permission.[23] Copyright 2020, The Authors, published by Wiley-VCH.
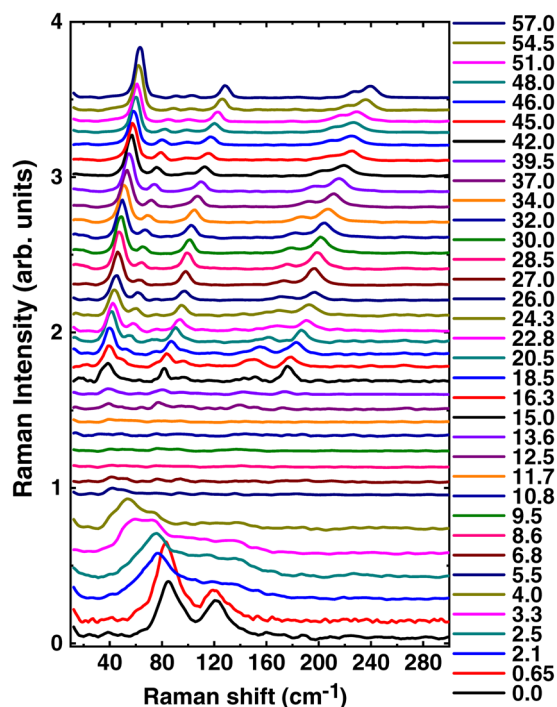
as the bandgap, the optical dielectric constant (ε_∞), and the Grüneisen parameter (γ_{TO}). The gradual change of the characteristic properties shown in Figure 8 is indicative for the reduction of metavalence upon increasing electron transfer. After PbS, a pronounced change is observed for all properties of β-PbO, suggesting a change in bonding type. Hence, the increased charge transfer and the concomitant change of properties clearly reveal an electron transfer-driven transition in chemical bonding. Changing the degree of electron transfer causes the weakening of MVB from PbTe to PbS and ultimately the loss of MVB in β-PbO.

4. MVB: Present Status and Future Perspectives

Besides the identification of metavalent bonds in further materials or even material classes, researchers have also made

successful attempts to induce or destroy MVB via external parameters. In this section, we will focus on relevant achievements related to MVB, stressing its potential in different fields.

High pressure has been a powerful tool to introduce subtle structure transitions. It enables the control of bonding and properties without changing the material composition. Pawbake and coworkers and Bellin and coworkers have reported pressure-dependent Raman studies of monochalcogenides including GeTe, GeSe, and SnSe.[58,66] The anomalous broadening and softening of the Raman modes observed in GeTe with both increased temperature and pressure (less than ≈15 GPa) have been related to MVB and its enhancement. The phonon frequency hardening in the high-pressure region (greater than ≈15 GPa), on the contrary, is associated with the electronic transition away from MVB, as shown in **Figure 9**.[58,66,67] The loss of MVB character with pressure has also been observed in

ADVANCED SCIENCE NEWS
www.advancedsciencenews.com

pssrrl
physica status solidi
www.pss-rapid.com

Figure 9. Raman spectra of GeTe from ambient pressure to 57 GPa in quasi-hydrostatic conditions. Reproduced with permission.[66] Copyright 2019, American Physical Society.
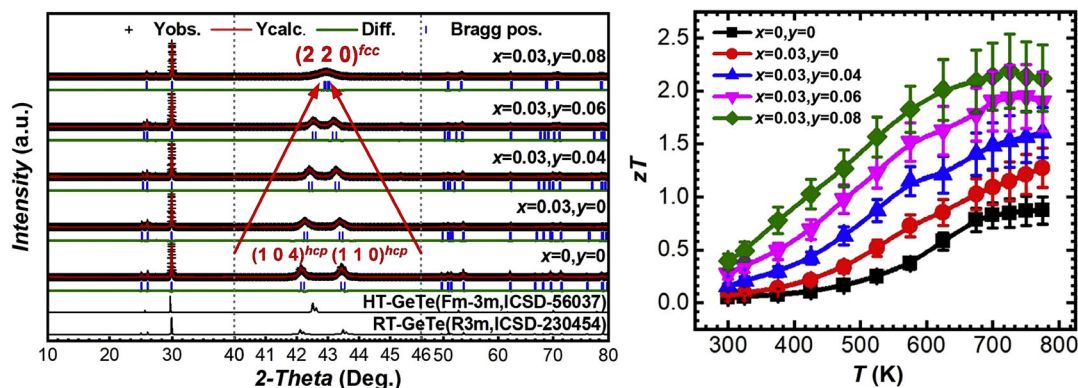
zincblende III–V compounds, a strong optical phonon softening results from the long-range electronic interaction of p-electrons. It leads to a large electron–phonon coupling and therefore strong anharmonicity in MVB materials.[29,31,48] The strong anharmonicity and consequently low-lattice thermal conductivity have been observed in many chalcogenides using MVB like SnTe and PbTe, ensuring fairly good thermoelectric performance even in pristine materials.[30,58,78–82] The long-range electronic interaction has also been demonstrated to be the origin of incipient ferroelectricity.[63] Besides thermal transport, MVB also leads to highly anisotropic band valleys which can increase the ratio of density of state effective mass and conductivity effective mass $\left(\frac{m_{\mathrm{DOS}}^*}{m_{\mathrm{Drude}}^*}\right)$ and thus enhances the power factor.[16,17,83–85] The manipulation of structural distortions and hence the MVB character of rhombohedral GeTe via doping has been demonstrated to be an effective route to promote thermoelectric performance.[15,86–88] As reported in a study by Li et al.,[15] the enhanced MVB properties induced by symmetrized GeTe lead to both ultrahigh peak and average ZT, as shown in **Figure 10**.

As a novel bonding mechanism primarily found in PCMs, MVB also reveals an intimate link with optical properties. As reported in a study by Koch et al.,[62] tailoring the strength of MVB via Se doping in $SnSb_2Te_4$ leads to a reduced absolute reflectivity and hence optical contrast between amorphous and crystalline phases. Besides the static optical properties, the femtosecond optical excitation of PCMs also reveals an ultrafast reduction of optical properties prior to amorphization.[59,61] This instantaneous optical change is due to the loss of MVB possibly triggered by the rattling motion of Ge atoms.[89,90] These observations are also technically important as they imply that the property contrast of PCMs may not necessarily require melting. Interestingly, besides the instantaneous loss of MVB, the metastable formation of metavalent bonds in some chalcogenide glasses upon an applied electrical field has been demonstrated to be responsible for the amorphous ovonic threshold switching (OTS) phenomenon.[91,92]

These studies demonstrate that manipulating and tailoring metavalent bonds provide a novel, promising route to property design. Given these and as well as lively discussions on the concept of MVB, additional advances are both desirable and should be rewarding. On the one hand, although ≈100 compounds have

SnSb$_2$Te$_4$ (≈2–4 GPa) and PbSe (≈3–4 GPa).[68–71] On the contrary, interestingly, in other p-bonded materials, GeSe and SnSe, the softening of some phonon modes with pressure has been linked with MVB.[58,72] A pressure-induced electronic transition toward MVB has also been observed in β-As$_2$S$_3$.[73] Particularly, this pressure-induced electronic transition or bonding transition results in the evolution of many properties characteristic for MVB including high Born effective charges, a moderate electrical resistivity, large optical dielectric constants, and small bandgaps.[68,74–77]

Recently, MVB has also emerged as a conceptually new route to advance the performance in thermoelectric materials. By comparing the lattice thermal conductivities of V$_2$VI$_3$ and IV–VI with

Figure 10. Left: Typical Rietveld-refined X-ray diffraction patterns of the sintered Ge$_{1-x}$Ti$_x$Te and Ge$_{0.97-y}$Ti$_{0.03}$Sb$_y$Te. Right: Temperature-dependent ZT of Ge$_{1-x-y}$Ti$_x$Sb$_y$Te. Reproduced with permission.[15] Copyright 2020, Elsevier.

ADVANCED
SCIENCE NEWS

www.advancedsciencenews.com

pss rrl
physica status solidi

www.pss-rapid.com

been included in the bonding map (Figure 4), a further extension toward a higher data density, possibly including ternary or even quaternary materials, is highly desirable. This could be very helpful, as many functional materials utilize more than just two elements. On the other hand, the borders between MVB and conventional bond types including covalent, ionic, and metallic bonding are still hardly addressed. This investigation should also be very beneficial as many application-related properties are highly dependent on the strength of MVB. It is thus rewarding to know in which composition range MVB can be expected.

5. Summary

Heavier chalcogenides provide significant potential for several applications of advanced functional materials, including PCMs, thermoelectrics, and topological insulators. This has motivated vivid discussions of the origin of their properties in the past decades. Studies of the type of chemical bonding used in this material class are potentially very rewarding as they provide efficient routes to design functional materials. Here we review the recent understanding of bonding in several families of heavier chalcogenides. The type of bonding utilized in three groups of chalcogenides has been discussed to reveal the underlying reason for their wide range of applications. Starting from IV–VI materials (GeTe, SnTe, PbTe, PbSe, and PbS), the unique property portfolio and bond-breaking behavior found in these materials have been demonstrated to be related to a novel chemical bonding mechanism termed "MVB." A similar property portfolio is also found for several V_2VI_3 solids (Bi_2Te_3, Bi_2Se_3, Sb_2Te_3, and β-As_2Te_3) and some ternary chalcogenides including crystalline $(GeTe)_{1-x}(Sb_2Te_3)_x$ alloys. The similarities between metavalently bonded IV–VI solids, the V_2VI_3 solids, and $(GeTe)_{1-x}(Sb_2Te_3)_x$ alloys point to the prevalence of MVB in these compounds. Then, a newly proposed electronic map using two quantum mechanical descriptors (ES and ET) has been presented. In this map, all different bonding mechanisms are located in well-separated regions. Materials using MVB are found in a region where about one electron is shared between adjacent atoms and a modest electron transfer occurs. The degree of MVB can be tailored either via Peierls distortions or charge transfer. The two approaches mainly affect either electron sharing between adjacent atoms or electron transfer and lead to the transitions toward covalent bonding and ionic bonding, respectively. As many technologically relevant properties of these materials rely on the strength of MVB, the tailoring of bonding provides a novel, promising route to property design.

Acknowledgements

Conflict of Interest

The authors declare no conflict of interest.

Keywords

[1] N. Yamada, E. Ohno, N. Akahira, K. i. Nishiuchi, K. i. Nagata, M. Takao, *Jpn. J. Appl. Phys.* **1987**, *26*, 61.
[2] M. Chen, K. A. Rubin, R. W. Barton, *Appl. Phys. Lett.* **1986**, *49*, 502.
[3] N. Yamada, E. Ohno, K. Nishiuchi, N. Akahira, M. Takao, *J. Appl. Phys.* **1991**, *69*, 2849.
[4] G. W. Burr, B. N. Kurdi, J. C. Scott, C. H. Lam, K. Gopalakrishnan, R. S. Shenoy, *IBM J. Res. Dev.* **2008**, *52*, 449.
[5] W. Zhang, R. Mazzarello, M. Wuttig, E. Ma, *Nat. Rev. Mater.* **2019**, *4*, 150.
[6] S. W. Fong, C. M. Neumann, H.-S. P. Wong, *IEEE Trans. Electron Devices* **2017**, *64*, 4374.
[7] M. Wuttig, N. Yamada, *Nat. Mater.* **2007**, *6*, 824.
[8] M. Wuttig, H. Bhaskaran, T. Taubner, *Nat. Photonics* **2017**, *11*, 465.
[9] Q. Wang, E. T. F. Rogers, B. Gholipour, C.-M. Wang, G. Yuan, J. Teng, N. I. Zheludev, *Nat. Photonics* **2016**, *10*, 60.
[10] K. Biswas, J. He, I. D. Blum, C.-I. Wu, T. P. Hogan, D. N. Seidman, V. P. Dravid, M. G. Kanatzidis, *Nature* **2012**, *489*, 414.
[11] L. Hu, T. Zhu, X. Liu, X. Zhao, *Adv. Funct. Mater.* **2014**, *24*, 5211.
[12] X.-L. Shi, J. Zou, Z.-G. Chen, *Chem. Rev.* **2020**, *120*, 7399.
[13] W.-D. Liu, D.-Z. Wang, Q. Liu, W. Zhou, Z. Shao, Z.-G. Chen, *Adv. Energy Mater.* **2020**, *10*, 2000367.
[14] Y. Pei, X. Shi, A. LaLonde, H. Wang, L. Chen, G. J. Snyder, *Nature* **2011**, *473*, 66.
[15] M. Li, M. Hong, X. Tang, Q. Sun, W.-Y. Lyu, S.-D. Xu, L.-Z. Kou, M. Dargusch, J. Zou, Z.-G. Chen, *Nano Energy* **2020**, *73*, 104740.
[16] Y. Yu, M. Cagnoni, O. Cojocaru-Mirédin, M. Wuttig, *Adv. Funct. Mater.* **2019**, *30*, 1904862.
[17] M. Cagnoni, D. Führen, M. Wuttig, *Adv. Mater.* **2018**, *30*, 1801787.
[18] H. Zhang, C.-X. Liu, X.-L. Qi, X. Dai, Z. Fang, S.-C. Zhang, *Nat. Phys.* **2009**, *5*, 438.
[19] Y. Tanaka, Z. Ren, T. Sato, K. Nakayama, S. Souma, T. Takahashi, K. Segawa, Y. Ando, *Nat. Phys.* **2012**, *8*, 800.
[20] L. Pauling, *The Nature of the Chemical Bond*, 3rd edition, Cornell University Press, Ithaca, NY, USA **1960**.
[21] M. Wuttig, V. L. Deringer, X. Gonze, C. Bichara, J.-Y. Raty, *Adv. Mater.* **2018**, *30*, 1803777.
[22] B. J. Kooi, M. Wuttig, *Adv. Mater.* **2020**, *32*, 1908302.
[23] S. Maier, S. Steinberg, Y. Cheng, C.-F. Schön, M. Schumacher, R. Mazzarello, P. Golub, R. Nelson, O. Cojocaru-Mirédin, J.-Y. Raty, M. Wuttig, *Adv. Mater.* **2020**, *32*, 2005533.
[24] O. Gunnarsson, M. Calandra, J. E. Han, *Rev. Mod. Phys.* **2003**, *75*, 1085.
[25] J. H. Mooij, *Phys. Status Solidi A* **1973**, *17*, 521.
[26] K. Robinson, G. V. Gibbs, P. H. Ribbe, *Science* **1971**, *172*, 567.
[27] G. Lucovsky, R. M. White, *Phys. Rev. B* **1973**, *8*, 660.
[28] D. Lencer, M. Salinga, B. Grabowski, T. Hickel, J. Neugebauer, M. Wuttig, *Nat. Mater.* **2008**, *7*, 972.

[29] S. Lee, K. Esfarjani, T. Luo, J. Zhou, Z. Tian, G. Chen, *Nat. Commun.* **2014**, *5*, 3525.

[30] M. E. Manley, O. Hellman, N. Shulumba, A. F. May, P. J. Stonaha, J. W. Lynn, V. O. Garlea, A. Alatas, R. P. Hermann, J. D. Budai, H. Wang, B. C. Sales, A. J. Minnich, *Nat. Commun.* **2019**, *10*, 1928.

[31] O. Delaire, J. Ma, K. Marty, A. F. May, M. A. McGuire, M. H. Du, D. J. Singh, A. Podlesnyak, G. Ehlers, M. D. Lumsden, B. C. Sales, *Nat. Mater.* **2011**, *10*, 614.

[32] B. Gault, M. P. Moody, J. M. Cairney, S. P. Ringer, *Atom Probe Microscopy, Springer Series in Materials Science*, Vol. *160*, Springer, New York **2012**.

[33] M. Zhu, O. Cojocaru-Mirédin, A. M. Mio, J. Keutgen, M. Küpers, Y. Yu, J. Y. Cho, R. Dronskowski, M. Wuttig, *Adv. Mater.* **2018**, *30*, 1706735.

[34] P. B. Littlewood, *J. Phys. C: Solid State Phys.* **1979**, *12*, 4459.

[35] P. B. Littlewood, *J. Phys. C: Solid State Phys.* **1980**, *13*, 4855.

[36] K. Shportko, S. Kremers, M. Woda, D. Lencer, J. Robertson, M. Wuttig, *Nat. Mater.* **2008**, *7*, 653.

[37] M. Raghuwanshi, O. Cojocaru-Mirédin, M. Wuttig, *Nano Lett.* **2020**, *20*, 116.

[38] J.-Y. Raty, M. Schumacher, P. Golub, V. L. Deringer, C. Gatti, M. Wuttig, *Adv. Mater.* **2019**, *31*, 1806280.

[39] G. J. Snyder, E. S. Toberer, *Nat. Mater.* **2008**, *7*, 105.

[40] Y. Luo, J. Yang, Q. Jiang, L. Fu, Y. Xiao, W. Li, D. Zhang, Z. Zhou, Y. Cheng, *Nano Energy* **2015**, *15*, 709.

[41] Y. Cheng, O. Cojocaru-Mirédin, J. Keutgen, Y. Yu, M. Küpers, M. Schumacher, P. Golub, J. Y. Raty, R. Dronskowski, M. Wuttig, *Adv. Mater.* **2019**, *31*, 1904316.

[42] J. Yanez-Limon, J. González-Hernández, J. Alvarado-Gil, I. Delgadillo, H. Vargas, *Phys. Rev. B* **1995**, *52*, 16321.

[43] T. Abraham, C. Juhasz, J. Silver, J. D. Donaldson, M. J. K. Thomas, *Solid State Commun.* **1978**, *27*, 1185.

[44] A. C. Garcia-Castro, N. A. Spaldin, A. H. Romero, E. Bousquet, *Phys. Rev. B* **2014**, *89*, 104107.

[45] A. R. Oganov, M. J. Gillan, G. D. Price, *J. Chem. Phys.* **2003**, *118*, 10174.

[46] G. Lucovsky, R. M. Martin, E. Burstein, *Phys. Rev. B* **1971**, *4*, 1367.

[47] K. Novoselov, A. Mishchenko, A. Carvalho, A. C. Neto, *Science* **2016**, *353*, aac9439.

[48] Y.-S. Song, J. Kim, S.-H. Jhi, *Phys. Rev. Appl.* **2018**, *9*, 054044.

[49] J.-Y. Raty, M. Wuttig, *J. Phys. D: Appl. Phys.* **2020**, *53*, 234002.

[50] B. Huang, J. Robertson, *Phys. Rev. B* **2010**, *81*, 081204.

[51] J. Akola, R. O. Jones, *Phys. Rev. B* **2007**, *76*, 235201.

[52] J.-J. Kim, K. Kobayashi, E. Ikenaga, M. Kobata, S. Ueda, T. Matsunaga, K. Kifune, R. Kojima, N. Yamada, *Phys. Rev. B* **2007**, *76*, 115124.

[53] U. V. Waghmare, N. A. Spaldin, H. C. Kandpal, R. Seshadri, *Phys. Rev. B* **2003**, *67*, 125111.

[54] R. E. Peierls, *Quantum Theory of Solids, Oxford Classic Texts in the Physical Sciences*, Vol. *23*, Oxford University Press, London, UK **1955**.

[55] J.-P. Gaspard, *C. R. Phys.* **2016**, *17*, 389.

[56] J. K. Burdett, S. Lee, *J. Am. Chem. Soc.* **1983**, *105*, 1079.

[57] J. C. Phillips, *Bonds and Bands in Semiconductors*, Academic Press, London, UK **1973**.

[58] C. Bellin, A. Pawbake, L. Paulatto, K. Béneut, J. Biscaras, C. Narayana, A. Polian, D. J. Late, A. Shukla, *Phys. Rev. Lett.* **2020**, *125*, 145301.

[59] L. Waldecker, T. A. Miller, M. Rudé, R. Bertoni, J. Osmond, V. Pruneri, R. E. Simpson, R. Ernstorfer, S. Wall, *Nat. Mater.* **2015**, *14*, 991.

[60] H. Tanimura, S. Watanabe, T. Ichitsubo, *Adv. Funct. Mater.* **2020**, *30*, 2002821.

[61] P. Fons, H. Osawa, A. V. Kolobov, T. Fukaya, M. Suzuki, T. Uruga, N. Kawamura, H. Tanida, J. Tominaga, *Phys. Rev. B* **2010**, *82*, 041203.

[62] C. Koch, G. Schienke, M. Paulsen, D. Meyer, M. Wimmer, H. Volker, M. Wuttig, W. Bensch, *Chem. Mater.* **2017**, *29*, 9320.

[63] M. P. Jiang, M. Trigo, I. Savić, S. Fahy, É. D. Murray, C. Bray, J. Clark, T. Henighan, M. Kozina, M. Chollet, J. M. Glownia, M. C. Hoffmann, D. Zhu, O. Delaire, A. F. May, B. C. Sales, A. M. Lindenberg, P. Zalden, T. Sato, R. Merlin, D. A. Reis, *Nat. Commun.* **2016**, *7*, 12291.

[64] T. Siegrist, P. Jost, H. Volker, M. Woda, P. Merkelbach, C. Schlockermann, M. Wuttig, *Nat. Mater.* **2011**, *10*, 202.

[65] S. Wang, Y. Sun, J. Yang, B. Duan, L. Wu, W. Zhang, J. Yang, *Energy Environ. Sci.* **2016**, *9*, 3436.

[66] A. Pawbake, C. Bellin, L. Paulatto, K. Béneut, J. Biscaras, C. Narayana, D. J. Late, A. Shukla, *Phys. Rev. Lett.* **2019**, *122*, 145701.

[67] Z. Sun, J. Zhou, H.-K. Mao, R. Ahuja, *Proc. Natl. Acad. Sci. USA* **2012**, *109*, 5948.

[68] M. Xu, S. Jakobs, R. Mazzarello, J.-Y. Cho, Z. Yang, H. Hollermann, D. Shang, X. Miao, Z. Yu, L. Wang, M. Wuttig, *J. Phys. Chem. C* **2017**, *121*, 25447.

[69] J. A. Sans, R. Vilaplana, E. L. da Silva, C. Popescu, V. P. Cuenca-Gotor, A. Andrada-Chacón, J. Sánchez-Benitez, O. Gomis, A. L. J. Pereira, P. Rodríguez-Hernández, A. Muñoz, D. Daisenberger, B. García-Domene, A. Segura, D. Errandonea, R. S. Kumar, O. Oeckler, P. Urban, J. Contreras-García, F. J. Manjón, *Inorg. Chem.* **2020**, *59*, 9900.

[70] S. V. Ovsyannikov, V. V. Shchennikov, A. E. Kar'kin, B. N. Goshchitskii, *J. Phys.: Condens. Matter* **2005**, *17*, S3179.

[71] S. Wang, C. Zang, Y. Wang, L. Wang, J. Zhang, C. Childs, H. Ge, H. Xu, H. Chen, D. He, Y. Zhao, *Inorg. Chem.* **2015**, *54*, 4981.

[72] H. Yu, D. Gao, X. Wang, X. Du, X. Lin, W. Guo, R. Zou, C. Jin, K. Li, Y. Chen, *NPG Asia Mater.* **2018**, *10*, 882.

[73] V. P. Cuenca-Gotor, J. Á. Sans, O. Gomis, A. Mujica, S. Radescu, A. Muñoz, P. Rodríguez-Hernández, E. L. da Silva, C. Popescu, J. Ibañez, *Phys. Chem. Chem. Phys.* **2020**, *22*, 3352.

[74] S. Ovsyannikov, V. Shchennikov, S. V. Popova, A. Y. Derevskov, *Phys. Status Solidi B* **2003**, *235*, 521.

[75] S. Wang, J. Zhang, Y. Zhang, A. Alvarado, J. Attapattu, D. He, L. Wang, C. Chen, Y. Zhao, *Inorg. Chem.* **2013**, *52*, 8638.

[76] A. Onodera, I. Sakamoto, Y. Fujii, N. Mo, S. Sugai, *Phys. Rev. B* **1997**, *56*, 7935.

[77] J. Yan, F. Ke, C. Liu, L. Wang, Q. Wang, J. Zhang, G. Li, Y. Han, Y. Ma, C. Gao, *Phys. Chem. Chem. Phys.* **2016**, *18*, 5012.

[78] C. Li, J. Ma, H. Cao, A. May, D. Abernathy, G. Ehlers, C. Hoffmann, X. Wang, T. Hong, A. Huq, *Phys. Rev. B* **2014**, *90*, 214303.

[79] C. Li, O. Hellman, J. Ma, A. May, H. Cao, X. Chen, A. Christianson, G. Ehlers, D. Singh, B. Sales, *Phys. Rev. Lett.* **2014**, *112*, 175501.

[80] D. Morelli, V. Jovovic, J. Heremans, *Phys. Rev. Lett.* **2008**, *101*, 035901.

[81] A. Banik, T. Ghosh, R. Arora, M. Dutta, J. Pandey, S. Acharya, A. Soni, U. V. Waghmare, K. Biswas, *Energy Environ. Sci.* **2019**, *12*, 589.

[82] J. M. Skelton, S. C. Parker, A. Togo, I. Tanaka, A. Walsh, *Phys. Rev. B* **2014**, *89*, 205203.

[83] X. Chen, D. Parker, D. J. Singh, *Sci. Rep.* **2013**, *3*, 3168.

[84] M. Hong, J. Zou, Z.-G. Chen, *Adv. Mater.* **2019**, *31*, 1807071.

[85] Y. Pei, A. D. LaLonde, H. Wang, G. J. Snyder, *Energy Environ. Sci.* **2012**, *5*, 7963.

[86] M. Hong, Z.-G. Chen, L. Yang, Y.-C. Zou, M. S. Dargusch, H. Wang, J. Zou, *Adv. Mater.* **2018**, *30*, 1705942.

[87] J. Li, X. Zhang, Z. Chen, S. Lin, W. Li, J. Shen, I. T. Witting, A. Faghaninia, Y. Chen, A. Jain, L. Chen, G. J. Snyder, Y. Pei, *Joule* **2018**, *2*, 976.

[88] D. Wu, L.-D. Zhao, S. Hao, Q. Jiang, F. Zheng, J. W. Doak, H. Wu, H. Chi, Y. Gelbstein, C. Uher, *J. Am. Chem. Soc.* **2014**, *136*, 11412.

[89] E. Matsubara, S. Okada, T. Ichitsubo, T. Kawaguchi, A. Hirata, P. F. Guan, K. Tokuda, K. Tanimura, T. Matsunaga, M. W. Chen, N. Yamada, *Phys. Rev. Lett.* **2016**, *117*, 135501.

[90] T. Kawaguchi, K. Tokuda, S. Okada, M. Yabashi, T. Ichitsubo, N. Yamada, E. Matsubara, *Phys. Rev. B* **2020**, *101*, 060302.

[91] P. Noé, A. Verdy, F. d'Acapito, J.-B. Dory, M. Bernard, G. Navarro, J.-B. Jager, J. Gaudin, J.-Y. Raty, *Sci. Adv.* **2020**, *6*, eaay2830.

[92] J.-Y. Raty, P. Noé, *Phys. Status Solidi RRL* **2020**, *14*, 1900581.

[93] S. Kremers, Ph. D Thesis, I. Institute of Physics (IA), RWTH-Aachen **2009**.

[94] L. S. Lerner, *J. Phys. Chem. Solids* **1966**, *27*, 1.

[95] Y. Fujii, K. Tanaka, A. Kosuga, *Scr. Mater.* **2019**, *162*, 272.

[96] R. D. Tomlinson, E. Elliott, L. Haworth, M. J. Hampshire, *J. Cryst. Growth* **1980**, *49*, 115.

[97] H. T. Shaban, M. Mobarak, M. M. Nassary, *Physica B: Condens. Matter* **2007**, *389*, 351.

[98] V. Jovovic, J. P. Heremans, *Phys. Rev. B* **2008**, *77*, 245204.

Yudong Cheng received his B.Sc. (2013) and M.Eng. (2016) in materials science and is currently working as a Ph.D. student at I. Institute of Physics (IA), RWTH Aachen University. His research interests are phase-change materials and atom probe tomography, including the chemical bonding mechanism, optical, and electronic properties.

Sophia Wahl received her M.Sc. in experimental condensed matter physics from RWTH Aachen University, Germany (2019), where she is currently pursuing her Ph.D. in physics in the group of Matthias Wuttig at the I. Institute of Physics (IA). Her research activities are focused on the optical characterization of compound semiconductors to investigate the connection between optical properties and the chemical bonding mechanism.

Matthias Wuttig received his Ph.D. in physics in 1988 from RWTH Aachen/ Forschungszentrum Jülich. He was a visiting professor at several institutions including Lawrence Berkeley Laboratory, CINaM (Marseille), Stanford University, Hangzhou University, IBM Almaden, Bell Labs, DSI in Singapore, and the Chinese Academy of Sciences in Shanghai. In 1997, he was appointed full professor at RWTH Aachen. Since 2011, he has been heading a collaborative research center on resistively switching chalcogenides (SFB 917), funded by the DFG.